Acta Crystallographica Section F
Structural Biology and Crystallization Communications
ISSN 1744-3091

Crystallization and preliminary crystallographic study of carnosinase CN2 from mice

Tetsuo Yamashita,‡ Hideaki Unno, Sayuri Ujita, Hiroto Otani,‡ Nobuaki Okumura, Akiko Hashida-Okumura, Katsuya Nagai§ and Masami Kusunoki*

Institute for Protein Research, Osaka University, 3-2 Yamada-oka, Suita, Osaka 565-0871, Japan

‡ Current address: Research Institute for Microbial Diseases, Osaka University, 3-1 Yamada-oka, Suita, Osaka 565-0871, Japan.
§ Current address: Y. M. P. International Corporation, Nakajima Building, 4-12-17 Toyosaki, Kita-ku, Osaka, Osaka 531-0072, Japan.

Correspondence e-mail: kusunoki@protein.osaka-u.ac.jp

Received 21 April 2006
Accepted 29 August 2006

Mammalian tissues contain several histidine-containing dipeptides, of which L-carnosine is the best characterized and is found in various tissues including the brain and skeletal muscles. However, the mechanism for its biosynthesis and degradation have not yet been fully elucidated. Crystallographic study of carnosinase CN2 from mouse has been undertaken in order to understand its enzymatic mechanism from a structural viewpoint. CN2 was crystallized by the hanging-drop vapour-diffusion technique using PEG 3350 as a precipitant. Crystals were obtained in complex with either Mn^{2+} or Zn^{2+}. Both crystals of CN2 belong to the monoclinic space group $P2_1$ and have almost identical unit-cell parameters (a = 54.41, b = 199.77, c = 55.49 Å, β = 118.52° for the Zn^{2+} complex crystals). Diffraction data were collected to 1.7 and 2.3 Å for Zn^{2+} and Mn^{2+} complex crystals, respectively, using synchrotron radiation. Structure determination is ongoing using the multiple-wavelength anomalous diffraction (MAD) method.

1. Introduction

L-Carnosine (β-alanyl-L-histidine) and structurally related dipeptides such as homocarnosine (γ-aminobutyryl-L-histidine) and anserine (β-alanyl-*N*-methyl-L-methylhistidine) are distributed in a wide variety of vertebrate tissues (Bonfanti *et al.*, 1999). L-Carnosine is present at particularly high concentrations in mammalian skeletal muscles and brain, but its physiological functions remain to be determined. We have recently found that intracranial injection of L-carnosine suppresses 2-deoxy-D-glucose-induced hyperglycaemia and that this effect is suppressed by thioperamide, a histamine H3 antagonist (Yamano *et al.*, 2001). We have also found that L-carnosine decreases the blood-pressure levels of DOCA-salt hypertension rats (Niijima *et al.*, 2002). In addition, L-carnosine facilitates the activity of parasympathetic nerves innervating the pancreas and kidney, while it inhibits the activity of sympathetic nerves innervating the pancreas (Yamano *et al.*, 2001). Moreover, L-carnosine is thought to be released from muscles by physical activity (Nagai *et al.*, 2003). These findings suggest that L-carnosine regulates the autonomic nervous system by modulating the activities of histaminergic neurons in the brain and thus functions as a beneficial factor of physical activity in diabetes and hypertension.

L-Carnosine is synthesized from β-alanine and L-histidine by carnosine synthetase and is degraded by carnosinase. However, the molecular characteristics of these enzymes are as yet largely unknown. Recently, cDNAs encoding dipeptidases that can degrade L-carnosine (CN1 and CN2) have been reported (Teufel *et al.*, 2003). We have independently found a carnosine-degrading enzyme that matched the nucleotide sequence of CN2 in mouse brain (Otani *et al.*, 2005). These enzymes belong to the metalloproteinase M20 family and digest a wide range of peptides, including L-carnosine. Immunohistochemical analysis showed that CN2 is highly concentrated in the tuberomammillary nucleus of the hypothalamus, where the neuronal cell bodies of histaminergic neurons are located (Otani *et al.*, 2005). This raised the possibility that L-carnosine is degraded by CN2 to supply the substrate of the histamine-synthesizing enzyme histidine decarboxylase. CN2 requires Mn^{2+} for full activity, whereas CN2 in

Table 1
Statistics of X-ray diffraction data collection.

Values in parentheses are for the highest resolution shell.

	Mn^{2+} complex			Zn^{2+} complex			
Unit-cell parameters (Å, °)	a = 54.49, b = 199.18, c = 55.21, β = 118.92			a = 54.41, b = 199.77, c = 55.49, β = 118.52			
Space group	$P2_1$			$P2_1$			
Data set	Edge	Peak	Remote	High resolution	Edge	Peak	Remote
Wavelength (Å)	1.8941	1.8926	1.7926	1.000	1.2834	1.2827	1.2573
Resolution (Å)	50.0–2.8 (2.91–2.81)	50.0–2.8 (2.90–2.80)	50.0–2.3 (2.38–2.30)	50.0–1.7 (1.76–1.70)	50.0–1.8 (1.86–1.80)	50.0–1.8 (1.86–1.80)	50.0–1.8 (1.86–1.80)
Redundancy	7.3 (6.3)	7.4 (6.9)	6.6 (3.1)	5.0 (3.4)	7.0 (4.4)	6.9 (4.4)	7.0 (4.6)
No. of observed reflections	183799	186077	264160	545738	617481	618712	638696
No. of unique reflections	25204 (2534)	25248 (2390)	39799 (1412)	109231 (8405)	88807 (5360)	89035 (5495)	90757 (6112)
Completeness (%)	99.9 (99.1)	99.3 (94.4)	86.8 (30.9)	96.1 (74.4)	92.8 (56.1)	93.2 (57.5)	94.7 (63.8)
$I/\sigma(I)$	31.8 (6.4)	45.2 (15.6)	35.3 (3.4)	38.4 (2.8)	46.2 (5.4)	47.1 (6.3)	45.5 (5.0)
R_{sym}† (%)	6.9 (27.8)	5.9 (14.2)	5.8 (23.5)	3.8 (34.2)	4.0 (19.9)	4.1 (18.0)	4.2 (22.1)

† $R_{sym} = \sum_{hkl}\sum_i |I_i(hkl) - \langle I(hkl)\rangle| / \sum_{hkl}\sum_i I_i(hkl)$, where $I_i(hkl)$ is the ith intensity measurement of reflection hkl, including symmetry-related reflections, and $\langle I(hkl)\rangle$ is its average.

complex with Zn^{2+} has around 10% of the activity of CN2 in complex with Mn^{2+}.

We initiated crystallographic study of CN2 from mice in order to understand its enzymatic mechanism from a structural viewpoint. CN2 was crystallized by the hanging-drop vapour-diffusion technique using PEG 3350 as a precipitant. The most highly homologous protein to CN2 of known structure is the aminopeptidase PepV from *Lactobacillus delbrueckii* (Jozic *et al.*, 2002). Its sequence identity is only 17% and hence the molecular-replacement method is not promising. Two kinds of crystals were obtained, in complex with Mn^{2+} or Zn^{2+}; the presence of the metal ions was confirmed by XAFS (X-ray absorption fine structure) spectra. We collected diffraction data sets from both types of crystal for independent MAD phasing in order to determine the two crystal structures and to compare them.

2. Expression and purification

A cDNA encoding full-length CN2 was obtained by reverse transcriptase-polymerase chain reaction from mouse brain mRNA as previously described (Otani *et al.*, 2005) and subcloned into the *Eco*RI–*Sma*I sites of the pGEX 4T3 vector (Amersham Biosciences). CN2 protein fused with glutathione-*S*-transferase at the N-terminus was then induced in *Escherichia coli* strain BL21(DE3) pLysS in the presence of 1 m*M* IPTG and 2 m*M* $MnCl_2$ for 12–16 h at 298 K. The *E. coli* cells were collected and sonicated in buffer containing 25 m*M* Tris–HCl pH 7.4, 50 m*M* NaCl, 0.2 m*M* $MnCl_2$, 1 m*M* DTT. After centrifugation, the supernatant was mixed with glutathione-Sepharose beads (Amersham Biosciences), washed and incubated with thrombin (Amersham Biosciences) for 12–16 h. The soluble fraction was then applied onto a gel-filtration column (HiLoad 26/60 Superdex 200pg, Amersham Biosciences) and an anion-exchange column (HiTrap Q, Amersham Biosciences) and protein was eluted with a linear gradient of 50–750 m*M* NaCl in the same buffer. The buffer of the protein solution was changed to that for crystallization by ultrafiltration with Centriprep YM-30 (Millipore). The final product, after thrombin cleavage, represents the full-length CN2 sequence (SWISS-PROT code CPGL1_MOUSE) preceded by five residues (GSPNS) of the expression vector. The number of amino-acid residues including N-terminal artificial five residues is 480.

3. Crystallization

Preparation and crystallization of the CN2 Zn^{2+} and Mn^{2+} complexes were carried out in the same way. CN2 was crystallized using the hanging-drop vapour-diffusion method. Initial screening for crystallization conditions was performed using Crystal Screens 1 and 2 (Hampton Research). However, we were not able to obtain crystals.

Thermostable proteins have a tendency to crystallize more easily (Yamagata *et al.*, 2001). Because the denaturation temperature of a protein depends on the pH and the additives present in the protein solution, finding conditions that maximize a protein's denaturation temperature may be assumed to increase its crystallization potential. To search for conditions leading to good crystals, we measured the thermal denaturation temperatures of the protein using a differential scanning calorimeter (MicroCal VP-DSC) under various conditions by changing the pH and adding inhibitors and additives, the details of which will be described elsewhere. We describe the crystallization conditions obtained by the differential scanning calorimeter below.

2 µl protein solution (20 mg ml^{-1}) in buffer containing 25 m*M* Tris–HCl pH 7.4, 50 m*M* NaCl, 0.2 m*M* $MnCl_2$, 1 m*M* DTT and 30 m*M* bestatin (an inhibitor) was mixed with an equal volume of reservoir solution and was allowed to equilibrate against 0.5 ml of the reservoir solution at 293 K. Wing-shaped crystals were obtained using a reservoir solution containing 20%(*w*/*v*) PEG 3350 and 0.2 *M* KF. Crystal size and quality were further improved with a combination of macroseeding and microseeding techniques (Stura, 1999). As a result, single crystals of dimensions 0.4 × 0.2 × 0.1 mm were obtained in hanging drops using 20%(*w*/*v*) PEG 3350, 20%(*w*/*v*) glycerol, 0.2 *M* KF as the reservoir solution (Fig. 1). In order to remove an excess of Mn^{2+}, crystals were transferred to harvesting solution consisting of 20%(*w*/*v*) PEG 3350, 20%(*w*/*v*) glycerol, 0.2 *M* KF for 1 d prior to X-ray data collection.

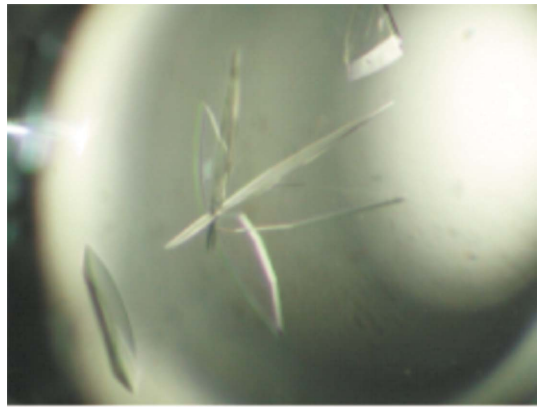

Figure 1
Crystals of mouse carnosinase.

4. Data collection and processing

Mn^{2+} and Zn^{2+} complex crystals of CN2 were mounted in nylon CryoLoops (Hampton Research) and placed directly into a nitrogen stream at 100 K. For identification of the metal type in the CN2 complex crystals, XAFS spectra were measured and used to discriminate the metal type. We selected crystals containing only Mn^{2+} or Zn^{2+} ions and used them for the Zn and Mn MAD method. Synchrotron-radiation oscillation data were collected using a Quantum 210 CCD detector (ADSC, USA) at beamline NW-12 of Photon Factory (KEK, Tsukuba, Japan) for a Mn^{2+} complex crystal at two wavelengths at the Mn *K* absorption edge of 1.8941 Å (edge) and 1.8926 Å (peak) and at one remote wavelength of 1.7926 Å; data were collected from a Zn^{2+} complex crystal at two wavelengths at the Zn *K* absorption edge of 1.2834 Å (edge), 1.2827 Å (peak) and two remote wavelengths of 1.000 and 1.2573 Å. Complete data sets were collected through contiguous rotation ranges at a given wavelength before proceeding to the next wavelength. The total oscillation ranges were 360° for all data collections except for the Zn high-resolution data set. Oscillation data were recorded in frames of 1° oscillation with 1 and 2 s exposures per image for Mn MAD and Zn MAD, respectively. One crystal was used for the Mn MAD data collection and one for the Zn MAD data collection. The data collected at the various wavelengths were processed with the program *HKL*-2000 (Otwinowski & Minor, 1997). Statistics of the MAD data sets are summarized in Table 1. The Mn complex crystal suffer appreciable radiation damage and its effects together with our data-collection conditions were reflected in the statistics. The space groups of all CN2 crystals were determined to be monoclinic $P2_1$. Assuming the presence of two molecules of CN2 in the asymmetric unit, the value of the Matthews coefficient V_M (Matthews, 1968) is 2.50 $Å^3$ Da^{-1}, corresponding to a solvent content of 49.9%, both of which are within the normal range of values for protein crystals (Matthews, 1968). The self-rotation function calculation showed strong peaks indicating twofold rotation symmetry. Structure analysis of the Zn^{2+} and Mn^{2+} complex crystals by MAD are currently in progress.

We are grateful to the beamline staff of Photon Factory BL12NW for their assistance during data collection. This research is supported by the National Project on Protein Structural and Functional Analyses from the Ministry of Education, Culture, Sports, Science and Technology of Japan. We are thankful to Dr Kyoko Ogasahara at the Institute for Protein Research, Osaka University and Dr Katsuhide Yutani at RIKEN SPring-8 Center, Harima Institute for the differential scanning calorimetry measurements and analysis.

References

Bonfanti, L., Peretto, P., De Marchis, S. & Fasolo, A. (1999). *Prog. Neurobiol.* **59**, 333–353.
Jozic, D., Bourenkow, G., Bartunik, H., Scholze, H., Dive, V., Henrich, B., Huber, R., Bode, W. & Maskos, K. (2002). *Structure*, **10**, 1097–1106.
Matthews, B. W. (1968). *J. Mol. Biol.* **33**, 491–497.
Nagai, K., Niijima, A., Yamano, T., Otani, H., Okumura, N., Tsuruoka, N., Nakai, M. & Kiso, Y. (2003). *Exp. Biol. Med.* **228**, 1138–1145.
Niijima, A., Okui, T., Matsumura, Y., Yamano, T., Tsuruoka, N., Kiso, Y. & Nagai, K. (2002). *Auton Neurosci.* **97**, 99–102.
Otani, H., Okumura, N., Okumura, A. & Nagai, K. (2005). *J. Biochem.* **137**, 167–175.
Otwinowski, Z. & Minor, W. (1997). *Methods Enzymol.* **276**, 307–326.
Stura, E. A. (1999). *Crystallization of Nucleic Acid and Proteins: A Practical Approach*, 2nd ed., edited by A. Ducruix & R. Giegé, pp. 177–208. Oxford University Press.
Teufel, M., Saudek, V., Ledig, J. P., Bernhardt, A., Boularand, S., Carreau, A., Cairns, N. J., Carter, C., Cowley, D. J., Duverger, D., Ganzhorn, A. J., Guenet, C., Heintzelmann, B., Laucher, V., Sauvage, C. & Smirnova, T. (2003). *J. Biol. Chem.* **278**, 6521–6531.
Yamagata, Y., Ogasahara, K., Hioki, Y., Lee, S. J., Nakagawa, A., Nakamura, H., Ishida, M., Kuramitsu, S. & Yutani, K. (2001). *J. Biol. Chem.* **276**, 11062–11071.
Yamano, T., Niijima, A., Iimori, S., Tsuruoka, N., Kiso, Y. & Nagai, K. (2001). *Neurosci. Lett.* **313**, 78–82.